PAPER • OPEN ACCESS

Influence of magnetic field alignment and defect concentration on nitrogen-vacancy polarization in diamond

To cite this article: M Drake *et al* 2016 *New J. Phys.* **18** 013011

New Journal of Physics
The open access journal at the forefront of physics

Deutsche Physikalische Gesellschaft DPG
IOP Institute of Physics

Published in partnership with: Deutsche Physikalische Gesellschaft and the Institute of Physics

OPEN ACCESS

RECEIVED
8 September 2015

REVISED
25 November 2015

ACCEPTED FOR PUBLICATION
10 December 2015

PUBLISHED
24 December 2015

PAPER

Influence of magnetic field alignment and defect concentration on nitrogen-vacancy polarization in diamond

M Drake[1], **E Scott**[2] **and J A Reimer**[1]

[1] Department of Chemical and Biomolecular Engineering, University of California, Berkeley, CA 94720, USA
[2] Department of Chemistry, University of California, Berkeley, CA 94720, USA

E-mail: drakem@berkeley.edu

Keywords: nitrogen-vacancy, P1 centers, NV centers, spin polarization, magnetic field alignment

Abstract

We present a quantitative, systematic study of the polarization of the Zeeman magnetic sublevels of the NV-defect in diamond as a function of magnetic field alignment relative to the NV-defect axis. The orientation dependence of NV-polarization in the lab frame is accounted for by a Wigner rotation of a constant defect frame polarization. We also find that the NV-defect level polarizations vary with the P1 defect concentration, and that the polarization of the $m_s = 0$ state with optical pumping decreases from 46% to 36% in samples as P1 concentrations vary from 20 ppm to 100 ppm, respectively.

Introduction

The negatively charged nitrogen vacancy center (NV-) is an electronic spin-1 defect in diamond consisting of a substitutional nitrogen, an adjacent carbon vacancy, and an electron donated from elsewhere in the lattice [1]. A difference in intersystem crossing rates between the $m_s = 0$ and $m_s = \pm 1$ excited state levels results in spin polarization into the $m_s = 0$ sublevel upon optical pumping [2]. NV-centers have applications in numerous fields, including magnetometry [3], nuclear spin polarization [4–12], and quantum information processing [13]. While many applications utilize single defects aligned with an applied magnetic field, understanding orientation dependence of NV-polarization is important for applications involving ensembles of defects in single crystals as well as defects in nanodiamonds. For example, significant bulk ^{13}C nuclear polarization has been measured in NV-doped diamonds subject to optical pumping of the ensemble of NV-defects at large (7 T) magnetic fields [5, 14]. The quantum mechanical processes that yield this nuclear hyperpolarization remain unclear, and modeling the phenomena likely requires an understanding of each NV-defect polarization at a given orientation to the field. Previous work shows the maximum NV-polarization occurs when the NV-defect axis is aligned with an applied magnetic field and has been observed to decrease with misalignment through spin dependent photoluminescence [2, 15] and defect-mediated nuclear polarization [4].

Polarization into the $m_s = 0$ sublevel can be quantified through a comparison of dark and optically illuminated EPR spectra [16, 17]. Here we use that method to study of the effect of magnetic field orientation on the polarization of the NV-Zeeman sub-levels. We further introduce a different method for calculating these polarizations that does not rely on assumptions about the relative magnitudes of $m_s = \pm 1$ polarization [16, 17]. The maximum NV-polarizations are compared across a number of samples with varying NV- and P1 defect concentrations.

Experimental methods

The sample used for the orientation study is an HPHT Type Ib diamond with a $\langle 100 \rangle$ out-of-plane orientation purchased from Element 6 and treated with 1 MeV electron irradiation (Prism Gem) and subsequently annealed at 800 °C for 2 h under 9%H/91%He gas flow. The sample was characterized previously [14] with an NV-concentration of 1.9 ± 0.2 ppm and a P1 concentration of 24 ± 3 ppm. X-ray diffraction was used to determine the in-plane crystal orientation to be $\langle 110 \rangle$ along the sample edges and $\langle 100 \rangle$ along the corners.

Table 1. Parameters used in EasySpin simulation of NV- and P1 X-band EPR spectrum.

Parameter	Value	Reference
g_{NV}	2.0028	Loubser and van Wyk [21]
g_{P1}	2.0024	Smith *et al* [22]
D_{NV}	2880 MHz	Loubser and van Wyk [21]
A_{P1}^{14N}	$A_\perp = 81$ MHz $A_\parallel = 115$ MHz	Smith *et al* [22]
A_{P1}^{13C}	$A_\perp = 141.8$ MHz $A_\parallel = 340.8$ MHz	Cox *et al* [23]

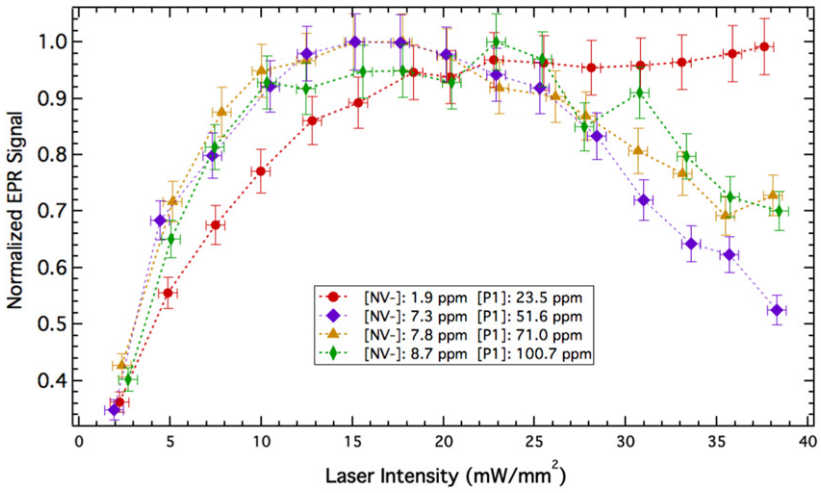

Figure 1. Normalized laser saturation curves for several diamonds via measured NV-EPR signals. Dashed lines are guides for the eye. Data acquired under illumination by a 532 nm laser with 5 mm beam diameter. Laser intensity was adjusted by increasing laser power from 50 to 750 mW. Red circle data points are from the diamond used in the NV polarization as a function of field alignment study. Defect concentrations were found using spin counting EPR techniques in a previous study [14].

The samples used to probe polarization as a function of defect concentration have also been characterized previously [14].

X-band CW EPR experiments were performed at room temperature with a modified Active Spectrum© extended range benchtop EPR system. Optical access to the sample was added perpendicular to the magnetic field direction by mounting a 45° mirror underneath an existing hole in the bottom of the microwave cavity. Samples were mounted on the end of a fiberglass rod cut at an angle that allowed one of the four NV-defect axes to be aligned with the field while exposing the large diamond face to the direction of laser propagation. The microwave power incident on the cavity was set to 0.001 58 mW. Spectra were recorded with 100 data points per mT using a conversion time of 100 ms, a modulation frequency of 43 kHz, and amplitude of 0.2 mT. Defect alignment relative to the magnetic field was adjusted by rotating the sample mount about the laser propagation axis (last step in figure 2(d)). Sample position relative to the field was determined by adjusting azimuthal and polar angles in an EasySpin simulation of the EPR spectrum until NV-peak positions matched those of the experimental spectrum [18]. A sample EPR spectrum and simulation overlay are depicted in figure 2(a). NV-parameters used in the EasySpin simulation are given in table 1. The symmetry of the diamond crystal dictates that for each orientation of a crystal axis in the magnetic field there will be four orientations of the NV-defect axis. Thus every EPR spectrum provides data for four unique defect orientations relative to the magnetic field. EasySpin simulations were also used to correctly assign the two transitions as $m_s = 0$ to $m_s = +1$ or $m_s = 0$ to $m_s = -1$, which change sides of the spectrum under certain orientations.

Spectra were acquired with (1 scan) and without (30 scans) 30.6 mW mm^{-2} of 532 nm circularly polarized laser light at each sample orientation. A laser saturation curve for several samples is shown in figure 1 and discussed in the context of NV-polarization as a function of defect concentration later in the manuscript. Using circularly polarized light and rotating the sample about the laser propagation axis allowed field alignment to be adjusted without introducing differences in laser absorption. The resulting spectra were fit to sums of first

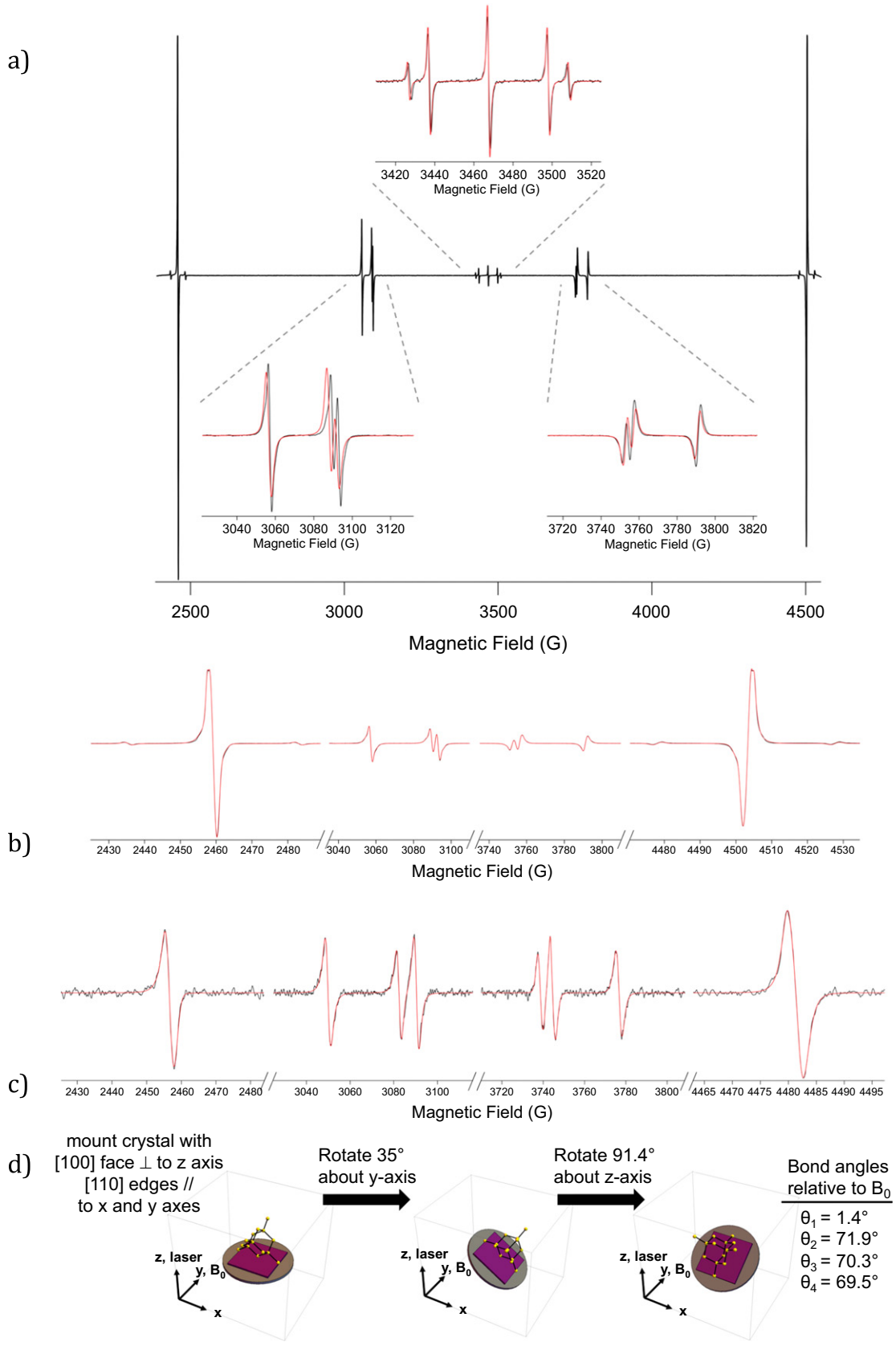

Figure 2. (a) Single scan X-band CW EPR spectrum under 30.6 mW mm^{-2} of 532 nm circularly polarized illumination (black) with insets of EasySpin simulation (red) using NV-angles relative to B_0 field of 1.4°, 71.9°, 70.3°, 69.5°. Sample orientation was manually adjusted in the simulation until best fit to the data. Central peaks emanate from the P1 centers. (b) NV-EPR peaks from (a) (black) fit to sums of Tsallian curves (red). (c) NV-EPR spectra (30 scans) without illumination (black) fit to sums of Tsallian curves (red). Spectra in (b) and (c) were acquired at the same orientation. Vertical axis in (c) is scaled 340x greater than in (b). (d) Crystal mounting procedure and final orientation relative to B_0 and the laser propagation axis for experimental data and corresponding simulations depicted in (a). Ball and stick model represents diamond lattice accurately oriented relative to the faces and edges of the diamond crystal (purple square). Gray circle represents bottom of sample mount used in the EPR cavity.

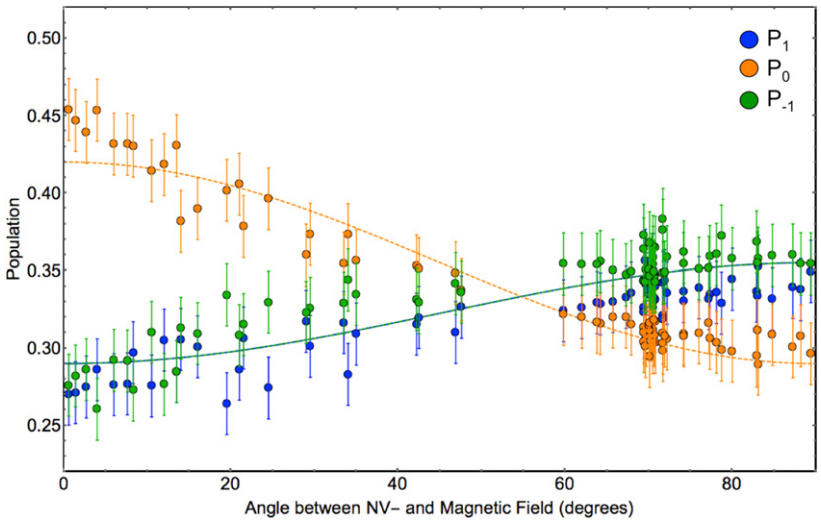

Figure 3. Polarization of NV-Zeeman eigenstates under 30.6 mW mm^{-2} of circularly polarized 532 nm illumination as determined from equations (1)–(3) and the X-band spectra. The lines represent calculated populations using Wigner rotations of the NV-bond-aligned polarizations into the lab frame.

derivative Tsallian lineshapes [19]. To avoid baseline problems and for more accurate results [20], double integration was carried out on line fits of the derivative spectra. An example EPR spectrum and fits are depicted in figures 2(b) and (c).

Populations of the three NV-eigenstates under illumination were calculated using the following set of equations (appendices A and B):

$$P_{+1,\mathrm{L}} = P_{0,\mathrm{L}} - (P_{0,\mathrm{D}} - P_{+1,\mathrm{D}})\frac{A_{+,\mathrm{L}}}{A_{+,\mathrm{D}}}\,, \tag{1}$$

$$P_{0,\mathrm{L}} = \frac{1}{3}\left[1 + (P_{0,\mathrm{D}} - P_{-1,\mathrm{D}})\frac{A_{-,\mathrm{L}}}{A_{-,\mathrm{D}}} + (P_{0,\mathrm{D}} - P_{+1,\mathrm{D}})\frac{A_{+,\mathrm{L}}}{A_{+,\mathrm{D}}}\right], \tag{2}$$

$$P_{-1,\mathrm{L}} = P_{0,\mathrm{L}} - (P_{0,\mathrm{D}} - P_{-1,\mathrm{D}})\frac{A_{-,\mathrm{L}}}{A_{-,\mathrm{D}}}\,, \tag{3}$$

where subscripts L and D represent light and dark experiments, respectively. The subscripts $+1$, 0, and -1 represent the corresponding NV-magnetic sublevel, and $+$ and $-$ represent the 0 to $+1$ and 0 to -1 NV-EPR transitions, respectively. P is the population of the energy level and A is the EPR double integral. Thermal populations in the dark were calculated from Boltzmann distributions using measured experimental temperatures and calculated energies at the experimental defect orientations.

NV polarization as a function of field alignment

Figure 3 shows the calculated NV-populations as a function of NV-bond axis angle relative to the magnetic field. When the magnetic field is aligned parallel to the NV-defect axis the derived population of the $m_s = 0$ state is 0.45 ± 0.02, in agreement with room temperature X-band values reported previously in the literature (0.42 ± 0.04) [16]. The populations of $m_s = \pm 1$ were confirmed to be equal within experimental error. Our error in the calculated NV-bond axis angle relative to the field is estimated to be within 0.5° based on multiple EasySpin fits to the same spectrum. Thus the error is approximately equal to the marker size in figure 3. To determine error in the calculated populations (± 0.02) shown in figure 3, multiple spectra were acquired at the same orientation, separately fit, and integrated. This error is perhaps best assessed from the spread in populations around 70° misalignment (figure 3). While the orientations were never exactly reproduced, we find a variation of approximately 0.04 in the clustering of data points.

Under perfect alignment of the NV-bond axis with the magnetic field, the lab frame and defect frame are identical and the Zeeman eigenstates are quantized along the defect axis. A Wigner rotation can be applied to this defect frame population to predict the lab frame population at a different orientation assuming the defect-frame population is independent of alignment (appendix A). The curves in figure 3 represent a fit to the data of a Wigner rotation of 0.42(0.29) aligned population for the $m_s = 0(\pm 1)$ states into the laboratory frame at various

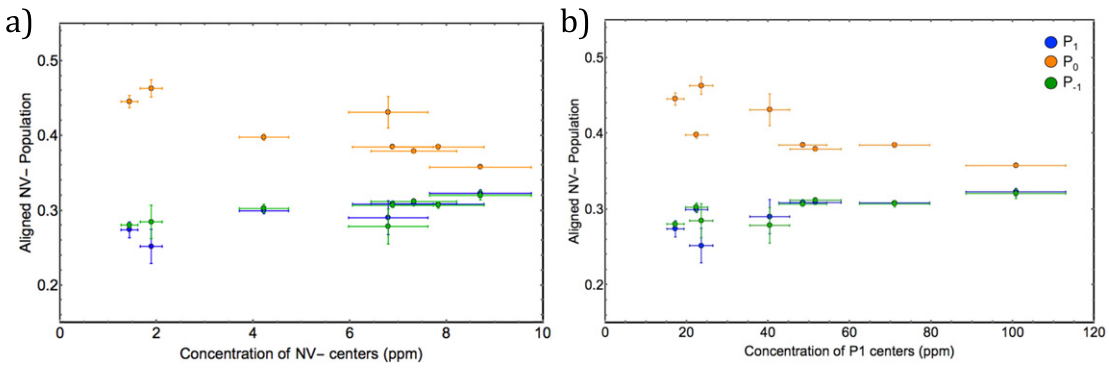

Figure 4. NV-polarizations as a function of (a) NV-concentration and (b) P1 concentration in Type 1b HPHT synthetic diamonds.

orientations. The reasonable fit to the data indicates that the defect-frame NV-polarization is constant as a function of defect misalignment with the field.

NV-polarization as a function of defect concentration

NV-polarizations of defects aligned with their bond axis parallel with magnetic field were measured for eight Type 1b HPHT diamonds with varying NV- and P1 (substitutional nitrogen) concentrations. Polarization was found to decrease with increasing NV-concentration as well as increasing P1 concentration, as seen in figure 4, but did not trend with the ratio of NV-to P1 concentrations (appendix C). Polarization into the $m_s = +1$ and $m_s = -1$ states were equal in all samples. The experiments were all performed at 30.56 mW mm^{-2} laser intensity, which falls on a different region of each sample's laser saturation curve as shown in figure 1. The samples with >7 ppm NV-were all past saturation at this intensity and would be expected to have larger polarizations at lower laser intensities based on figure 1. It is unexpected that higher NV-concentration samples saturated at lower laser intensities. Increased concentrations of P1 centers may decrease NV-polarization through increasing relaxation [24] or through facilitating NV-to NV^0 photo-ionization [25–27]. Photo-ionization increases with laser intensity [25–27], and may explain the observed laser saturation trends. Additional studies of the influence of laser intensity on NV-polarization using a larger sample pool with greater variation in defect concentrations are needed to further understand these observed trends.

The significant increase in NV-polarization with decreasing P1 concentration is consistent with previously observed optically pumped nuclear polarizations in these samples at high magnetic fields [7]. Only samples with approximately 20 ppm P1 centers had observable ^{13}C polarization at room temperature and 7 and 9.4 T fields.

Summary and conclusions

We have presented a systematic study of NV-polarization as a function of magnetic field orientation relative to the NV-bond axis and defect concentration. NV-polarizations were found to be constant in the defect frame at X-band field strengths. The experimentally observed orientation dependence was fully accounted for by a Wigner rotation of the NV-bond axis frame into the laboratory frame. NV-polarization of the $m_s = +1$ and $m_s = -1$ states were confirmed to be equal using a straightforward method for separately calculating their polarizations. NV-polarization of aligned defects was found to trend with NV- and P1 concentrations, but not their ratio. Polarization into $m_s = 0$ varied from 46% to 36% in samples where P1 concentrations varied from 20 to 100 ppm, respectively, and NV-concentrations varied from 1.4–9 ppm,

These results affirm the use of constant Zeeman level polarizations in the defect frame for all orientations of the NV-defect relative to the magnetic field. This magnetic field orientation independence is an important consideration for applications utilizing ensembles of defects in single crystals and defects in nanodiamonds. Further, the significant increase in NV-polarization in diamonds with lower P1 concentrations provides a design metric for future sample optimization for applied spin technologies.

Acknowledgments

The authors thank Dr Arturas Vailionis for assisting in the x-ray diffraction work to determine the in-plane orientations of our samples. We also thank Active Spectrum for assisting in modifications to their standard

MicroESR system. MD acknowledges support from an NSF Graduate Research Fellowship under Grant No. DGE 1106400. The initial portions of this work were supported by the National Science Foundation through Grant No. NSF-1106288. Publication was made possible in part by support from the Berkeley Research Impact Initiative (BRII) sponsored by the UC Berkeley Library.

Appendix A. Rotating the Hamiltonian into the lab frame

Wigner rotations were used to rotate Hamiltonian terms into the same reference frame. The NV-center Hamiltonian is composed of three terms, representing the Zeeman interaction, the zero field splitting interaction, and crystal strain. For this paper, we chose to put all interactions into the laboratory frame, which we define as having a z-axis parallel to the applied B_0 field of the X-band EPR apparatus. The traditional Zeeman term interaction ($\gamma B_0 S_z$) is therefore already in the correct frame. However, the zero field splitting ($D(S_z{}^2\text{–}S(S+1)/3)$) and crystal strain ($E(S_+{}^2+S_-{}^2)$) terms are represented in the defect frame and need to be rotated into the laboratory frame.

We first represent the terms as spherical tensors ($\hat{T}_\mu{}^{(\omega)}$), where ω is the rank of the tensor. We then determine the Wigner Rotation ($D_{q\mu}{}^{(\omega)}$) needed to transform the tensor into the new basis, which is defined by the relationship:

$$R\hat{T}_\mu^{(\omega)}R^{-1}=\sum_{q=-\omega}^{\omega}D_{q\mu}^{(\omega)}T_q^{(\omega)}. \tag{A.1}$$

We use the secular approximation that $q=0$ because only $T_0{}^{(2)}$ commutes with the Zeeman term. Both the zero field splitting and crystal strain terms are rank 2. Based on the change in angular momentum induced by the spin operators, it is easy to see that the zero field splitting and crystal strain terms belong to $\mu=0$ and $\mu=\pm2$, respectively

$$D\left(S_z^2-\frac{S(S+1)}{3}\right)\rightarrow D(\hat{T}_0^{(2)}), \tag{A.2}$$

$$R\hat{T}_0^{(2)}R^{-1}=\sum_{q=-2}^{2}D_{q0}^{(2)}T_q^{(2)}=D_{00}^{(2)}T_0^{(2)}=\left(\frac{3\cos^2\theta-1}{2}\right)T_0^{(2)}, \tag{A.3}$$

$$E(S_+^2+S_-^2)\rightarrow E(\hat{T}_{\pm2}^{(2)}), \tag{A.4}$$

$$R\hat{T}_{\pm2}^{(2)}R^{-1}=\sum_{q=-2}^{2}D_{q2}^{(2)}T_q^{(2)}=D_{02}^{(2)}T_0^{(2)}=\left(\sqrt{\frac{3}{8}}\sin^2\theta\right)T_0^{(2)}. \tag{A.5}$$

The NV-Hamiltonian in the laboratory frame is then:

$$H=\gamma B_0 S_Z+D\left(\frac{3\cos^2\theta-1}{2}\right)\left(S_z^2-\frac{S(S+1)}{3}\right)+E\left(\sqrt{\frac{3}{8}}\sin^2\theta\right)(S_+^2+S_-^2). \tag{A.6}$$

The following expressions relate the laboratory-frame populations (P_{+1}, P_0, P_{-1}) to the defect-frame populations (P'_{+1}, P'_0, P'_{-1}), through a Wigner Rotation

$$P_{+1}=\mathrm{d}(\theta)_{11}^2P'_{+1}+\mathrm{d}(\theta)_{01}^2P'_0+\mathrm{d}(\theta)_{-11}^2P'_{-1}, \tag{A.7}$$

$$P_0=\mathrm{d}(\theta)_{10}^2P'_{+1}+\mathrm{d}(\theta)_{00}^2P'_0+\mathrm{d}(\theta)_{-10}^2P'_{-1}, \tag{A.8}$$

$$P_{-1}=d(\theta)_{1-1}^2P'_{+1}+d(\theta)_{0-1}^2P'_0+d(\theta)_{-1-1}^2P'_{-1}. \tag{A.9}$$

Appendix B. Derivation of polarization equations

Equations (1)–(3) in the main text were derived by rearranging equations (B.1)–(B.3). Given the experimental restriction of operating in the linear regime of the power saturation curve, the double integral of the dispersive EPR line shapes is proportional to the population difference of the states involved in the transition. Equations (B.1) and (B.2) relate the ratios of population differences to EPR signal area for each of the NV-transitions. Equation (B.3) states that the fractional populations must add up to unity

$$\frac{P_{0,\mathrm{L}}-P_{+1,\mathrm{L}}}{A_{+,\mathrm{L}}}=\frac{P_{0,\mathrm{D}}-P_{+1,\mathrm{D}}}{A_{+,\mathrm{D}}}, \tag{B.1}$$

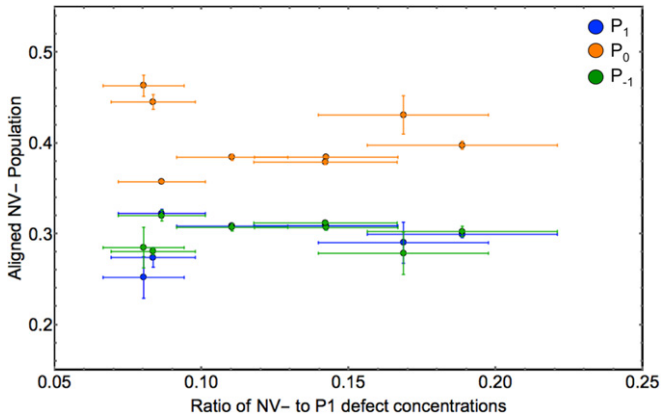

Figure C.1. NV-polarizations as a function of the ratio of NV- to P1 concentrations in Type 1b HPHT synthetic diamonds.

$$\frac{P_{0,\mathrm{L}} - P_{-1,\mathrm{L}}}{A_{-,\mathrm{L}}} = \frac{P_{0,\mathrm{D}} - P_{-1,\mathrm{D}}}{A_{-,\mathrm{D}}}, \tag{B.2}$$

$$P_{+1,\mathrm{L}} + P_{0,\mathrm{L}} + P_{-1,\mathrm{L}} = 1. \tag{B.3}$$

Appendix C. Lack of trend for NV-polarization as a function of [NV-]/[P1]

Figure C.1 shows the same NV- population data from figure 4 of the main text plotted as a function of the ratio of NV- and P1 concentrations. One might expect that the NV-polarization would be greater as the ratio of [NV-]/[P1] is increased due to greater distances between NV- and P1 and therefore decreased interactions leading to relaxation and photoionization, but that was not observed.

References

[1] Doherty M W, Manson N B, Delaney P, Jelezko F, Wrachtrup J and Hollenberg L C L 2013 The nitrogen-vacancy colour centre in diamond *Phys. Rep.* **528** 1–45
[2] Tetienne J-P, Rondin L, Spinicelli P, Chipaux M, Debuisschert T, Roch J-F and Jacques V 2012 Magnetic-field-dependent photodynamics of single NV defects in diamond: an application to qualitative all-optical magnetic imaging *New J. Phys.* **14** 103033
[3] Hong S, Grinolds M S, Pham L M, Le Sage D, Luan L, Walsworth R L and Yacoby A 2013 Nanoscale magnetometry with NV centers in diamond *MRS Bull.* **38** 155–61
[4] Jacques V, Neumann P, Beck J, Markham M, Twitchen D, Meijer J, Kaiser F, Balasubramanian G, Jelezko F and Wrachtrup J 2009 Dynamic polarization of single nuclear spins by optical pumping of nitrogen-vacancy color centers in diamond at room temperature *Phys. Rev. Lett.* **102** 057403
[5] King J P, Coles P J and Reimer J A 2010 Optical polarization of ^{13}C nuclei in diamond through nitrogen vacancy centers *Phys. Rev.* B **81** 1–4
[6] Wang H-J, Shin C S, Avalos C E, Seltzer S J, Budker D, Pines A and Bajaj V S 2013 Sensitive magnetic control of ensemble nuclear spin hyperpolarization in diamond *Nat. Commun.* **4** 1940
[7] Fischer R, Bretschneider C O, London P, Budker D, Gershoni D and Frydman L 2013 Bulk nuclear polarization enhanced at room temperature by optical pumping *Phys. Rev. Lett.* **111** 057601
[8] Fischer R, Jarmola A, Kehayias P and Budker D 2013 Optical polarization of nuclear ensembles in diamond *Phys. Rev.* B **87** 125207
[9] Smeltzer B, McIntyre J and Childress L 2009 Robust control of individual nuclear spins in diamond *Phys. Rev.* A **80** 050302
[10] Álvarez G A, Bretschneider C O, Fischer R, London P, Kanda H, Onoda S, Isoya J, Gershoni D and Frydman L 2015 Local and bulk ^{13}C hyperpolarization in nitrogen-vacancy-centred diamonds at variable fields and orientations *Nat. Commun.* **6** 8456
[11] Pagliero D, Laraoui A, Henshaw J D and Meriles C A 2014 Recursive polarization of nuclear spins in diamond at arbitrary magnetic fields *Appl. Phys. Lett.* **242402** 0–5
[12] King J P, Jeong K, Vassiliou C C, Shin C S, Page R H, Avalos C E, Wang H-J and Pines A 2015 Room-temperature *in situ* nuclear spin hyperpolarization from optically pumped nitrogen vacancy centers in diamond *Nat. Commun.* **6** 8965
[13] Childress L and Hanson R 2013 Diamond NV centers for quantum computing and quantum networks *MRS Bull.* **38** 134–8
[14] Scott E, Drake M and Reimer J A 2015 Optically pumped ^{13}C NMR in diamond at 7.05 T *J. Magn. Reson.* in press
[15] Epstein R J, Mendoza F M, Kato Y K and Awschalom D D 2005 Anisotropic interactions of a single spin and dark-spin spectroscopy in diamond *Nat. Phys.* **1** 94–8
[16] Felton S, Edmonds A, Newton M, Martineau P, Fisher D, Twitchen D and Baker J 2009 Hyperfine interaction in the ground state of the negatively charged nitrogen vacancy center in diamond *Phys. Rev.* B **79** 075203
[17] Harrison J, Sellars M J and Manson N B 2006 Measurement of the optically induced spin polarisation of N-V centres in diamond *Diam. Relat. Mater.* **15** 586–8
[18] Stoll S and Schweiger A 2006 EasySpin, a comprehensive software package for spectral simulation and analysis in EPR *J. Magn. Reson.* **178** 42–55

[19] Howarth D F, Weil J A and Zimpel Z 2003 Generalization of the lineshape useful in magnetic resonance spectroscopy *J. Magn. Reson.* **161** 215–21
[20] Tseitlin M, Eaton S S and Eaton G R 2012 Uncertainty analysis for absorption and first-derivative electron paramagnetic resonance spectra *Concepts Magn. Reson.* A **40A** 295–305
[21] Loubser J H N and van Wyk J A 1978 Electron spin resonance in the study of diamond *Rep. Prog. Phys.* **41** 1201–48
[22] Smith W V, Sorokin P P, Gelles I L and Lasher G J 1959 Electron-spin resonance of nitrogen donors in diamond *Phys. Rev.* **115** 1546–53
[23] Cox A, Newton M E and Baker J M 1994 ^{13}C, ^{14}N and ^{15}N ENDOR measurements on the single substitutional nitrogen centre (P1) in diamond *J. Phys.: Condens. Matter* **6** 551–63
[24] Takahashi S, Hanson R, van Tol J, Sherwin M and Awschalom D 2008 Quenching spin decoherence in diamond through spin bath polarization *Phys. Rev. Lett.* **101** 047601
[25] Aslam N, Waldherr G, Neumann P, Jelezko F and Wrachtrup J 2013 Photo-induced ionization dynamics of the nitrogen vacancy defect in diamond investigated by single-shot charge state detection *New J. Phys.* **15** 013064
[26] Manson N B and Harrison J P 2005 Photo-ionization of the nitrogen-vacancy center in diamond *Diam. Relat. Mater.* **14** 1705–10
[27] Gaebel T *et al* 2005 Photochromism in single nitrogen-vacancy defect in diamond *Appl. Phys.* B **82** 243–6